Real-time displacement measurement with a two-wavelength sinusoidal phase-modulating laser diode interferometer

Takamasa Suzuki, Katsuyuki Kobayashi, and Osami Sasaki

A two-wavelength interferometer that uses two separate modulating currents with different phases but the same frequencies to detect a greater degree of object displacement in real time is proposed and demonstrated. The measurement error was 57 nm, roughly 1/80 of the synthetic wavelength. We have confirmed that this modulating technique enables us to equip our prototype interferometer with a simple feedback-control system that eliminates external disturbance. © 2000 Optical Society of America

OCIS codes: 120.3180, 120.5050, 120.5060, 140.2020.

1. Introduction

Wavelength multiplexing in interferometry was proposed in the early days of holographic interferometry[1] as a means of eliminating phase ambiguity. In a two-wavelength interferometer[2] (TWI) the large synthetic wavelength $\lambda_s = \lambda_1\lambda_2/|\lambda_1 - \lambda_2|$ is able to remove the phase ambiguity that is introduced by the original shorter wavelengths λ_1 and λ_2. Many other kinds of TWI, for instance, the phase-shifting interferometer,[3,4] the speckle interferometer,[5] and the heterodyne interferometer,[6] have been proposed. Among other more recently developed varieties are those that utilize two different laser diodes (LD's), each with its own fine-tunable wavelength, such as the scanning spot interferometer,[7] the heterodyne interferometer,[8] the phase-shifting interferometer,[9,10] and the sinusoidal phase-modulating interferometer.[11]

Generally in TWI's, two mixed signals are registered simultaneously by a single photodetector. The simplest and most commonly used method of estimating phase in TWI is to calculate the difference between the phases that are obtained for the two original wavelengths used in the optical setup.[11] This kind of TWI, however, detects each phase separately, complicating the measurement in real time of the phase that corresponds to the synthetic wavelength.

We propose, therefore, a TWI that detects the phase difference in real time. In phase modulation, we use sinusoidal signals whose frequencies are the same but whose initial phases are not. As outlined in what follows, our approach is different from the method described in Ref. 11, in which sinusoidal modulating signals of different frequencies were used. The use of interference signals modulated with the same frequency simplifies signal processing. First, as the interference signals vary with the same frequency, the detected wave form, which is obtained as a sum of two interference signals, is simple and does not require a wideband photodetector. Second, a feedback signal for the elimination of external disturbance can easily be generated. We have confirmed that our TWI enables us to stabilize the interference signal with a simple feedback system.

2. Device Configuration and Operation

A. Optical System

Figure 1 depicts the setup of the TWI. The combined light from two LD's is fed into a Twyman–Green interferometer, which consists of mirrors M2 and M3 and beam splitter BS2. The difference in the lengths of the two arms is defined as D_0. Mirror M3 is mounted upon a piezoelectric transducer (PZT) and displaced by distance $d(t)$ along the optical axis. The interference signal is detected by a photodetector (PD). dc bias current, modulating current, and feedback current $I_c(t)$ for the LD are mixed by a LD modulator (LM) and injected into each LD. I_1 and I_2

The authors are with the Faculty of Engineering, Niigata University, 8050 Ikarashi 2, Niigata 950-2181, Japan.

Received 18 October 1999; revised manuscript received 2 February 2000.

0003-6935/00/162646-07$15.00/0

© 2000 Optical Society of America

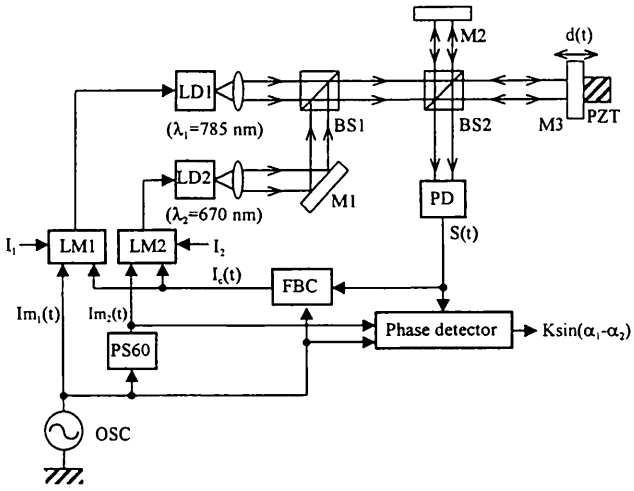

Fig. 1. Schematic of the experimental setup: M's, mirrors; OSC, oscillator; other abbreviations defined in text.

represent the dc bias currents employed. Modulating currents

$$I_{m_i}(t) = m_i \cos(\omega_c t + \theta_i) \qquad (i = 1, 2) \tag{1}$$

for LD1 and LD2 have the same frequency, but their amplitudes and phases are different. The interference signals generated by the laser beam from LD1 and LD2 are given by

$$S_i(t) = a_i + b_i \cos[z_i \cos(\omega_c t + \theta_i) + \alpha_i(t) + \delta_i(t)] \quad (i = 1, 2), \tag{2}$$

where

$$z_i = 4\pi m_i \beta_i [D_0 + d(t)]/\lambda_i^2, \tag{3}$$

$$\alpha_i(t) = 4\pi[D_0 + d(t)]/\lambda_i, \tag{4}$$

and $\delta_i(t)$ are modulation depths, phases determined by the optical path difference (OPD) $2[D_0 + d(t)]$, and phase changes caused by external disturbance, respectively. β_i represents modulation efficiency of the LD.

B. Displacement Measurement

To simplify the explanation we neglect $\delta_i(t)$ in the following formulas. If displacement $d(t)$ is larger than λ_i, it cannot be accurately detected with a single wavelength. We can, however, detect $d(t)$ without ambiguity if the phase difference

$$\Delta\alpha(t) = \alpha_1(t) - \alpha_2(t) = (4\pi D_0/\Lambda) + [4\pi d(t)/\Lambda] \tag{5}$$

is measured in a TWI, where

$$\Lambda = \lambda_1\lambda_2/|\lambda_1 - \lambda_2| \tag{6}$$

is a synthetic wavelength. Temporal displacement $d(t)$ is then given by

$$d(t) = \frac{\Lambda}{4\pi}\Delta\alpha(t), \tag{7}$$

as the first term of Eq. (5) is constant.

Because we use just one photodetector, the interference signal that it detects is given by

$$S(t) = \sum_i S_i(t). \tag{8}$$

To detect phase difference $\Delta\alpha(t)$ from the signal shown in Eq. (8), we made a phase detector. A block diagram of the phase detector is shown in Fig. 2. In the front end of the phase detector, the four signals

$$g_i(t) = m_i \sin(\omega_c t + \theta_i), \tag{9}$$

$$h_i(t) = I_{m_i}(t) \times g_i(t) = (m_i^2/2)\sin 2(\omega_c t + \theta_i) \tag{10}$$

are generated. We easily generate the signals shown in Eq. (9) by delaying the phase of the modulating current by $\pi/2$ with phase shifters PS90. Signals $h_i(t)$ are generated by use of multipliers (MUL's). We use synchronous detection[12] to extract the desired signals. Multiplying $S(t)$ and $g_1(t)$ and eliminating higher-frequency components with a low-pass filter (LPF), we extract the signal

$$S_{g_1}(t) = -b_2 m_1 J_1(z_2)\sin(\theta_1 - \theta_2)\sin\alpha_2(t) \tag{11}$$

(see Appendix A).

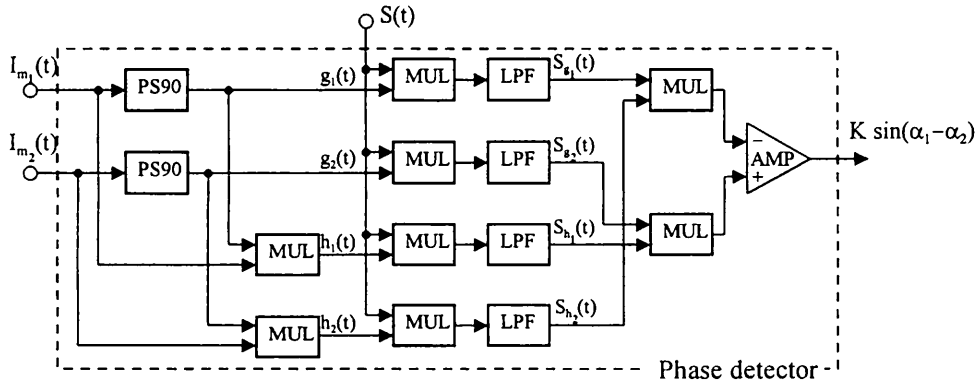

Fig. 2. Block diagram of the phase detector: AMP, differential amplifier; other abbreviations defined in text.

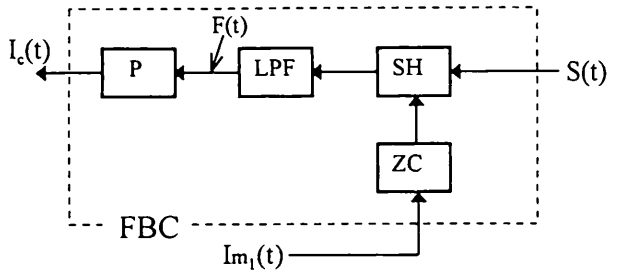

Fig. 3. Block diagram of the FBC: $F(t)$, feedback signal; other abbreviations defined in text.

In the same manner, by multiplying $S(t)$ by g_2, h_1, and h_2, we obtain

$$S_{g_2}(t) = -b_1 m_2 J_1(z_1)\sin(\theta_1 - \theta_2)\sin\alpha_1(t), \quad (12)$$

$$S_{h_1}(t) = -[b_2 m_1^2 J_2(z_2)/2]\sin 2(\theta_1 - \theta_2)\cos\alpha_2(t), \quad (13)$$

$$S_{h_2}(t) = -[b_1 m_2^2 J_2(z_1)/2]\sin 2(\theta_1 - \theta_2)\cos\alpha_1(t), \quad (14)$$

where $J_n(z_i)$ is the nth-order Bessel function. Taking the product of Eqs. (11) and (14) and that of Eqs. (12) and (13), we obtain

$$S_{g_1}(t) \times S_{h_2}(t) = U_1 m_1 m_2^2[b_1 b_2 J_1(z_2)J_2(z_1)/2] \times C\cos\alpha_1(t)\sin\alpha_2(t), \quad (15)$$

$$S_{g_2}(t) \times S_{h_1}(t) = U_2 m_1^2 m_2[b_1 b_2 J_1(z_1)J_2(z_2)/2] \times C\sin\alpha_1(t)\cos\alpha_2(t), \quad (16)$$

where

$$C = \sin(\theta_1 - \theta_2)\sin 2(\theta_1 - \theta_2) \quad (17)$$

and U_1 and U_2 are gains of the multipliers positioned at the latter part of the phase detector. By adjusting amplitudes m_1 and m_2 of the modulating current we can realize the condition $J_1(z)J_2(z) = J_1(z_1)J_2(z_2) = J_1(z_2)J_2(z_1)$. By adjustment of gains U_1 and U_2 such that $A = U_1 m_1 m_2^2 = U_2 m_1^2 m_2$, the amplitudes of the signals shown in Eqs. (15) and (16) assume the same value. Then, subtracting Eq. (15) from Eq. (16) with a differential amplifier, we can elicit sinusoidal signal $S_{\Delta\alpha}(t)$, which contains phase difference $\Delta\alpha$ as Eq. (18):

$$S_{\Delta\alpha}(t) = S_{g_2}(t) \times S_{h_1}(t) - S_{g_1}(t) \times S_{h_2}(t) = K\sin\Delta\alpha(t), \quad (18)$$

where

$$K = (A/2)b_1 b_2 C J_1(z)J_2(z) \quad (19)$$

is a constant. We then extract phase difference $\Delta\alpha(t)$ directly from Eq. (18). Consequently, from Eqs. (7) and (18), the displacement is given by

$$d(t) = \frac{\Lambda}{4\pi}\sin^{-1}\left[\frac{S_{\Delta\alpha}(t)}{K}\right]. \quad (20)$$

C. Elimination of the External Disturbance

This TWI can include a simple feedback controller (FBC) to eliminate external disturbance. The basic theory of how to eliminate the external disturbance has already been described.[13] We detect $\delta_i(t)$, the phase change caused by the external disturbance, as an argument of a sinusoidal function. This signal is used as a feedback signal. The FBC keeps this feedback signal constant by variation of the wavelength of the LD.

Because LD1 and LD2 share frequencies of the modulating current, the frequencies of the interference signals $S_1(t)$ and $S_2(t)$ obtained with respect to LD1 and LD2, respectively, are almost the same. Moreover, $\delta_1(t)$ and $\delta_2(t)$ are almost the same because they are generated in the same interferometer and λ_1/λ_2, the ratio of the wavelengths, is ~1.17. These facts allow us to use the sum of the two interference signals to generate the feedback signal.

A block diagram of the FBC is shown in Fig. 3. Zero-crossing circuit ZC generates a periodic sampling pulse train that has a constant interval of $2\pi/\omega_c$ at the electrical zero level of the modulating current $Im_1(t)$. $S(t)$ is sampled and held with a sample-and-hold circuit (SH). Higher-frequency components of the signal from the sample-and-hold circuit are removed by the LPF. If the object is not subjected to vibration, the feedback signal $F(t)$ is given by

$$F(t) = a_1 + a_2 + b_1\cos[\alpha_1 + \delta_1(t)] + b_2\cos[z_2\sin(\theta_1 - \theta_2) + \alpha_2 + \delta_2(t)], \quad (21)$$

where

$$\alpha_i = 4\pi D_0/\lambda_i \qquad (i = 1, 2). \quad (22)$$

The temporal signal that contributes to the elimination of external disturbance is

$$F(t) \approx \sum_i k_i b_i \delta_i(t) \qquad (0 < k_i < 1), \quad (23)$$

where k_1 and k_2 are the coefficients that are determined by the constant phases α_1 and $z_2\sin(\theta_1 - \theta_2) + \alpha_2$, respectively, at the operating point.[14] This feedback signal is relayed to proportional controller P, which then generates the control current $I_c(t)$. As shown in Fig. 1, the FBC system is constructed in such a way as to allow control current $I_c(t)$ to feed directly to LD1 and LD2. The wavelengths of LD1 and LD2 vary by $\Delta\lambda_1 = \beta_1 I_c(t)$ and $\Delta\lambda_2 = \beta_2 I_c(t)$, respectively. The controlled interference signal is then given by

$$S_{FB}(t) = \left\{\sum_i a_i + b_i\cos[z_i\cos(\omega_c t + \theta_i) + \alpha_i + \delta_i(t) - \alpha_{c_i}(t)]\right\}, \quad (24)$$

where FB means feedback and

$$\alpha_{c_i} = (4\pi D_0/\lambda_i^2)\Delta\lambda_i \quad (25)$$

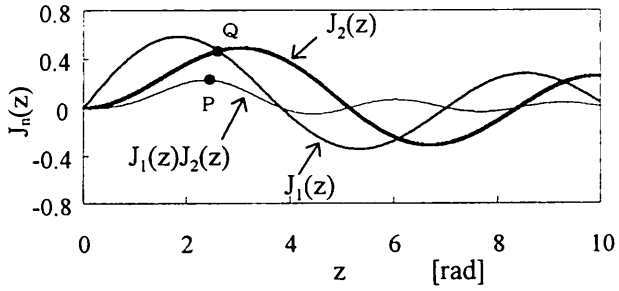

Fig. 4. Calculation of the Bessel functions $J_1(z)$, $J_2(z)$, and $J_1(z)J_2(z)$ with respect to modulation depth z. $J_1(z)J_2(z)$ takes its maximum at point P. $J_1(z)$ and $J_2(z)$ take the same values at point Q, which is very close to point P.

is a compensating phase introduced by the feedback control.[14]

3. Experimental Setup

The experimental setup is shown in Fig. 1. The initial OPD, $2D_0$, was 200 mm in our experiment. The wavelengths of LD1 and LD2 were 785 and 670 nm, respectively. Synthetic wavelength Λ then became 4.57 μm. The maximum measurable range was $\Lambda/2$ = 2.3 μm. Sinusoidal signal $\mathrm{Im}_1(t)$, the frequency $\omega_c/2\pi$ of which is 20 kHz, was used as a fundamental modulating current. The phase of $\mathrm{Im}_1(t)$ was shifted by 60° by phase shifter PS60 to generate $\mathrm{Im}_2(t)$. The phase difference between the two modulating currents was then 60°, as explained below in Section 4. Amplitudes m_1 and m_2 of the modulating currents were 0.36 and 0.16 mA, respectively. Because modulation efficiencies β_1 and β_2 were gauged to be 3.61×10^{-3} and 5.92×10^{-3} nm/mA with respect to LD1 and LD2, respectively, modulation depths z_1 and z_2 were then 2.58 and 2.65 rad, in that order. Then, the values of the Bessel function, $J_1(z_1)$, $J_1(z_2)$, $J_2(z_1)$, and $J_2(z_2)$, similarly become 0.476, 0.457, 0.457, and 0.465, respectively.

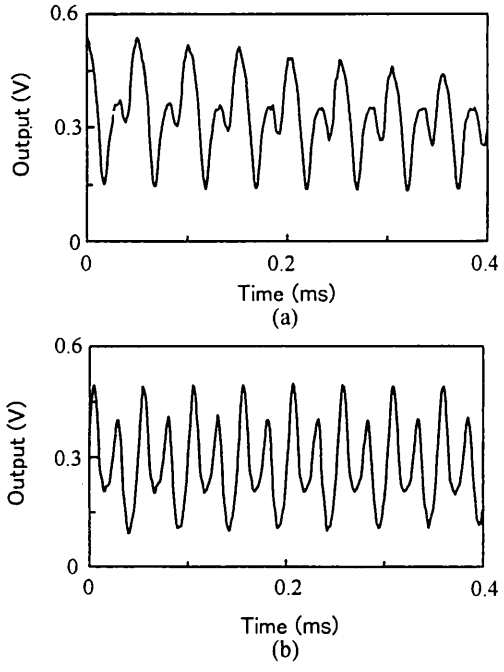

Fig. 5. Interference signals observed by the photodetector (a) without feedback control and (b) with feedback control.

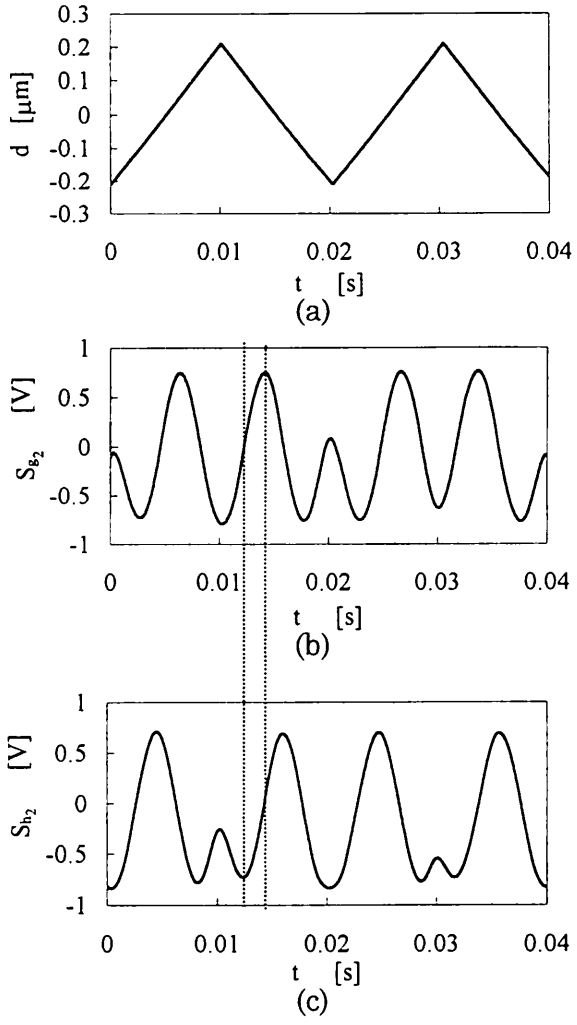

Fig. 6. Illustration of the extracted quadratic signals with respect to (a) the triangular displacement of mirror M3. The phase difference between signals (b) S_{g_2} and (c) S_{h_2} is $\pi/2$.

In the phase detector shown in Fig. 2, the cutoff frequencies of all LPF's were set to 200 Hz to remove useless higher-frequency components completely. These LPF's limit the detectable displacement frequency to no more than 100 Hz.

4. Optimum Measuring Conditions

To improve the signal-to-noise ratio, it is necessary to maximize K from Eq. (19). We examined the parameters of $J_1(z)J_2(z)$ and C in coefficient K. Figure 4 shows the theoretical values of $J_1(z)$, $J_2(z)$, and $J_1(z)J_2(z)$. $J_1(z)J_2(z)$ takes its maximum value of z = 2.39 rad at point P. In our experiments, however, we set z to be 2.63 rad at point Q. In doing this we simplified the overall adjustment, which enabled us to set signal $J_1(z)J_2(z)$ easily near the maximum point.

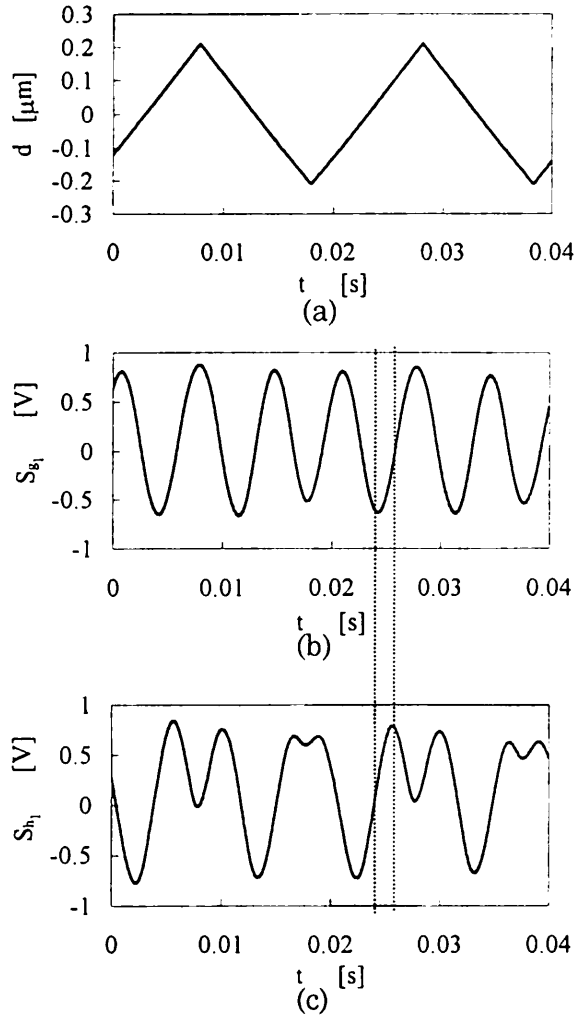

Fig. 7. Illustration of the extracted quadratic signals with respect to (a) the triangular displacement of mirror M3. The phase difference between signals (b) S_{g_1} and (c) S_{h_1} is $\pi/2$.

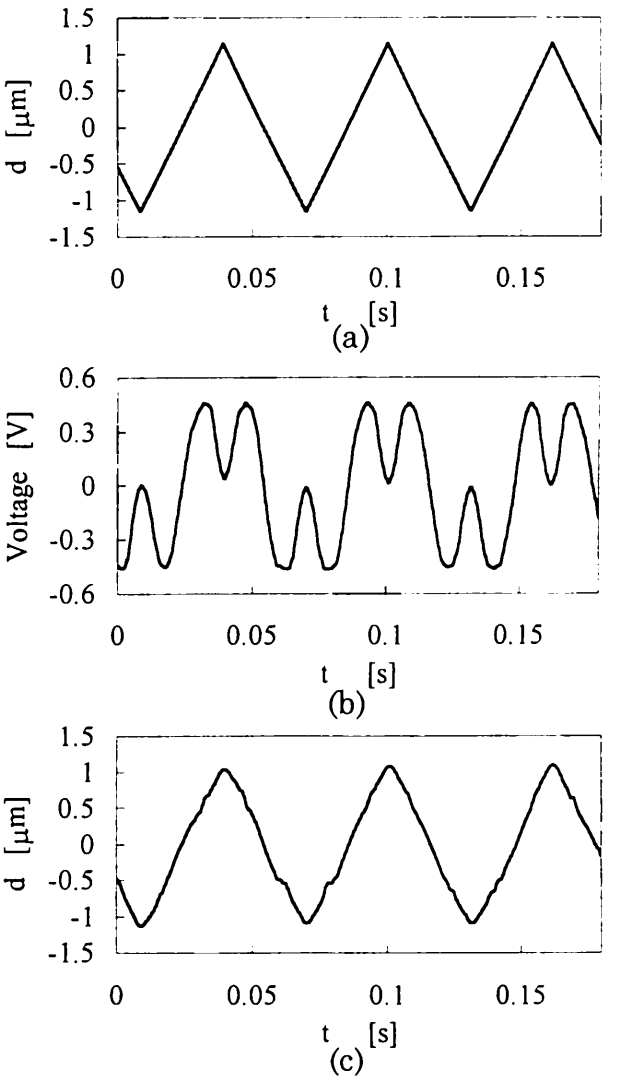

Fig. 8. Measurement of the large triangular displacement: (a) the displacement of mirror M3, (b) the output signal from the phase detector, (c) the displacement measured with the help of computer.

Although C achieves its maximum value at a phase difference $\theta_1 - \theta_2$ of 54.7°, we set the phase difference at 60° because its adjustment is simply easier at that level and because values for C differ little from 54.7° to 60° (see Appendix B).

Coefficient K contains Bessel functions $J_1(z)$ and $J_2(z)$. As modulation depth z is a function of the OPD, as shown in Eq. (3), K varies with the displacement $d(t)$ of the object. We can estimate the variations of $J_1(z)$ and $J_2(z)$ with respect to the change of the OPD by calculating

$$\frac{\partial J_i(z)}{\partial z}\Delta z \qquad (i = 1, 2). \tag{26}$$

Coefficients $\partial J_i(z)/\partial z$ are obtained as -0.29 and 0.11 near $z = 2.63$ for $i = 1$ and $i = 2$, respectively, with numerical calculations. Taking the maximum measurable range of 2.3 μm into account, we can estimate a maximum Δz of 6.05×10^{-5} by calculating Eq. (3). Consequently, the variations of $J_1(z)$ and $J_2(z)$ are -1.76×10^{-5} and 6.66×10^{-6}, respectively, which indicates that K remains constant even if the OPD changes to $\Lambda/2$. That is, even if $J_1(z)$ and $J_2(z)$ fluctuate, the overall integrity of the measurement is maintained.

5. Experimental Results

First, we measured the effect of feedback control by observing interference signal $S(t)$. In this experiment, the PZT did not vibrate. Because the modulating frequency was 20 kHz, the cutoff frequency of the LPF in the FBC was set to 2 kHz. $S(t)$ observed without feedback control is shown in Fig. 5(a). As slow or otherwise generally undesirable phase changes induced by external disturbances are superimposed upon $S(t)$, the waveform varied gradually. Such phase changes were completely eliminated in $S(t)$ observed with feedback control in the operation, as shown in Fig. 5(b). These results confirm that a conventional feedback-control system can easily and

effectively be applied to our TWI. When we install a feedback-control mechanism in vibration measurements, however, we have to equip our system with another interferometer that detects only external disturbance. Because our prototype setup does not have such an interferometer, there was no feedback control in the part of the experiment described below.

Next we observed the extracted quadratic signals represented by Eqs. (11)–(14). In this segment of the experiment the PZT was driven by triangular voltage to alter the phase, such that the waveform was as is shown in Fig. 6. The displacement of mirror M3 shown in Fig. 6(a) was calculated from the applied voltage for the PZT. Figures 6(b) and 6(c) illustrate the signals of S_{g_2} and S_{h_2}, respectively. We can confirm that they are proportional to $\sin \alpha_1$ and $\cos \alpha_1$, because the value of $\cos \alpha_1$ is lowest when $\sin \alpha_1$ crosses zero and the phase difference is $\pi/2$. The same observations were made for signals S_{g_1} and S_{h_1} as well. The displacement of M3 is shown in Fig. 7(a). Signals S_{g_1} and S_{h_1}, which are proportional to $\sin \alpha_2$ and $\cos \alpha_2$, respectively, are shown in Figs. 7(b) and 7(c). The phase difference between these signals was $\pi/2$. The results shown in Figs. 6 and 7 indicate that with our modulating technique quadratic signals can be extracted from the sum of two different interference signals.

Finally, real-time detection of the phase difference was demonstrated. The results are shown in Fig. 8. The PZT vibrated with a triangular signal, as shown in Fig. 8(a). The displacement of mirror M3 was 2.25 μm, which was equivalent to half of synthetic wavelength Λ. The final output, $S_{\Delta\alpha}(t) = K \sin \Delta\alpha(t)$ [see Eq. (18)], is traced in Fig. 8(b). The phase change of $S_{\Delta\alpha}(t)$ is easily estimated as 2π in the linear part of the triangular displacement. This result confirms that the signal of the trigonometric function that contains phase difference $\Delta\alpha = \alpha_1 - \alpha_2$ is directly obtained by our method. Figure 8(c) shows the amount of vibration of M3. This waveform was obtained from the signal shown in Fig. 8(b) through a computer calculation of Eq. (20). The waveforms shown in Figs. 8(a) and 8(c) agree well. The measurement error calculated on the linear part of the waveform was 57 nm rms. If we use a semiconductor device that can calculate trigonometric functions, such as Analog Devices Model AD639, an actual real-time displacement measurement can be made.

6. Conclusions

We have proposed and demonstrated a TWI that uses a novel modulating technique. The modulating currents of its LD's each have a unique phase but the same frequency in this technique. The device enables us to separate two phases that are generated with respect to two LD's and to implement feedback control to eliminate external disturbance with a simple feedback system. For purposes of the present research we were able to measure the overall displacement, the amplitude of which exceeded the measurable range of a conventional single-wavelength interferometer. But, for actual real-time measurements to be made, the final stage of the signal processing will have to be done without a computer.

Appendix A

Using the Bessel function, we rewrite interference signals $S_1(t)$ and $S_2(t)$ as

$$S_1(t) = a_1 + b_1\{\cos \alpha_1[J_0(z_1) - 2J_2(z_1)\cos 2(\omega_c t + \theta_1) + \cdots] - \sin \alpha_1[2J_1(z_1)\cos(\omega_c t + \theta_1) - 2J_3(z_1)\cos 3(\omega_c t + \theta_1) + \cdots]\}, \quad \text{(A1)}$$

$$S_2(t) = a_2 + b_2\{\cos \alpha_2[J_0(z_2) - 2J_2(z_2)\cos 2(\omega_c t + \theta_2) + \cdots] - \sin \alpha_2[2J_1(z_2)\cos(\omega_c t + \theta_2) - 2J_3(z_2)\cos 3(\omega_c t + \theta_2) + \cdots]\}. \quad \text{(A2)}$$

Taking the product of $S(t)$ and $g_1(t)$, we generate the dc component by the multiplication of two signals of the same frequency. The dc component can be extracted with a LPF. Taking note of the $S(t)$ components that have same frequency as $g_1(t)$, we can obtain

$$-2b_1J_1(z_1)\sin \alpha_1 \cos(\omega_c t + \theta_1) \times m_1 \sin(\omega_c t + \theta_1) = -b_1m_1J_1(z_1)\sin \alpha_1 \sin 2(\omega_c t + \theta_1), \quad \text{(A3)}$$

$$-2b_2J_1(z_2)\sin \alpha_2 \cos(\omega_c t + \theta_2) \times m_1 \sin(\omega_c t + \theta_1) = -b_2m_1J_1(z_2)\sin \alpha_2[\sin(2\omega_c t + \theta_1 + \theta_2) + \sin(\theta_1 - \theta_2)] \quad \text{(A4)}$$

with respect to $S_1(t)$ and $S_2(t)$, respectively. Because the product

$$\cos[k(\omega_c t + \theta_i)] \times \sin[k(\omega_c t + \theta_j)] = \frac{[\sin(2k\omega_c t + \theta_i + \theta_j) + \sin(\theta_i - \theta_j)]}{2} \quad (k = 1, 2), \quad \text{(A5)}$$

generates the dc component of $(1/2)\sin(\theta_i - \theta_j)$ when $i \neq j$, the dc component in the signal given in Eq. (A4) remains as shown in Eq. (11), whereas the signal given in Eq. (A3) is removed if we use a LPF. The other components in $S(t)$ whose frequencies are not equal to that of $g_1(t)$ are also eliminated with the LPF.

Appendix B

Putting $\theta_1 - \theta_2 = x$, we can obtain

$$f(x) = \sin x \sin 2x = 2 \sin^2 x \cos x. \quad \text{(B1)}$$

Differentiating Eq. (B1) gives us

$$f'(x) = 2 \sin x(2 - 3 \sin^2 x). \quad \text{(B2)}$$

When $\sin x = 0$ or $\sin x = \sqrt{2/3}$, $f'(x)$ becomes zero. Then the maximum of $f(x)$ is 0.7698 at $x = 54.7°$. $f(x)$, however, takes almost the maximum, 0.75, at $x = 60°$.

References

1. J. C. Wyant, "Testing aspherics using two-wavelength holography," Appl. Opt. **10,** 2113–2118 (1971).
2. C. Polhemus, "Two-wavelength Interferometry," Appl. Opt. **12,** 2071–2074 (1973).
3. Y.-Y. Cheng and J. C. Wyant, "Two-wavelength phase shifting interferometry," Appl. Opt. **23,** 4539–4543 (1984).
4. K. Creath, "Step height measurement using two-wavelength phase-shifting interferometry," Appl. Opt. **26,** 2810–2816 (1987).
5. A. F. Fercher, H. Z. Hu, and U. Vry, "Rough surface interferometry with a two-wavelength heterodyne speckle interferometer," Appl. Opt. **24,** 2181–2188 (1985).
6. Z. Sodnik, E. Fischer, T. Ittner, and H. J. Tiziani, "Two-wavelength double heterodyne interferometry using a matched grating technique," Appl. Opt. **30,** 3139–3144 (1991).
7. A. J. den Boef, "Two-wavelength scanning spot interferometer using single-frequency diode lasers," Appl. Opt. **27,** 306–311 (1988).
8. C. C. Williams and K. Wickramasinghe, "Absolute optical ranging with 200-nm resolution," Opt. Lett. **14,** 542–544 (1989).
9. Y. Ishii and R. Onodera, "Two-wavelength laser-diode interferometry that uses phase-shifting techniques," Opt. Lett. **16,** 1523–1525 (1991).
10. R. Onodera and I. Yukihiro, "Two-wavelength phase-shifting interferometry insensitive to the intensity modulation of dual laser diodes," Appl. Opt. **33,** 5052–5061 (1994).
11. O. Sasaki, H. Sasazaki, and T. Suzuki, "Two-wavelength sinusoidal phase/modulating laser-diode interferometer insensitive to external disturbances," Appl. Opt. **30,** 4040–4045 (1991).
12. T. Suzuki, O. Sasaki, S. Takayama, and T. Maruyama, "Real-time displacement measurement using synchronous detection in a sinusoidal phase modulating interferometer," Opt. Eng. **32,** 1033–1037 (1993).
13. O. Sasaki, K. Takahashi, and T. Suzuki, "Sinusoidal phase modulating laser diode interferometer with a feedback control system to eliminate external disturbance," Opt. Eng. **29,** 1511–1515 (1990).
14. T. Suzuki, T. Okada, O. Sasaki, and T. Maruyama, "Real-time vibration measurement using a feedback type of laser diode interferometer with an optical fiber," Opt. Eng. **36,** 2496–2502 (1997).